

AD-A068 767

NIELSEN ENGINEERING AND RESEARCH INC MOUNTAIN VIEW CALIF F/G 20/4  
A TRANSONIC WIND TUNNEL INTERFERENCE ASSESSMENT - AXISYMMETRIC --ETC(U)  
JAN 79 S S STAHARA, J R SPREITER F44620-75-C-0047

UNCLASSIFIED

AFOSR-TR-79-0627

NL

| OF |  
AD  
A068 767



END  
DATE  
FILMED

6 --79  
DDC

1. REPORT DOCUMENTATION PAGE		2. GOVT ACCESSION NO.		3. RECIPIENT'S CATALOG NUMBER	
18 AFOSR-TR-79-0627					
4. TITLE (and Subtitle)		5. TYPE OF REPORT & PERIOD COVERED			
A TRANSONIC WIND TUNNEL INTERFERENCE ASSESSMENT - AXISYMMETRIC FLOWS		INTERIM rept.			
7. AUTHOR(s)		6. PERFORMING ORG. REPORT NUMBER			
S S STAHARA		79-0203			
J.R./Spreiter		9. CONTRACT OR GRANT NUMBER(s)			
		F44620-75-C-0047, DAAG29-77-C-0038			
9. PERFORMING ORGANIZATION NAME AND ADDRESS		10. PROGRAM ELEMENT, PROJECT, TASK AREA & WORK UNIT NUMBERS			
NIELSEN ENGINEERING & RESEARCH, INC		2307A1			
510 CLYDE AVE		61102F			
MOUNTAIN VIEW, CA 94043					
11. CONTROLLING OFFICE NAME AND ADDRESS		12. REPORT DATE			
AIR FORCE OFFICE OF SCIENTIFIC RESEARCH/NA		11 Jan 79			
BLDG 410		13. NUMBER OF PAGES			
BOLLING AIR FORCE BASE, D C 20332		9			
14. MONITORING AGENCY NAME & ADDRESS (if different from Controlling Office)		15. SECURITY CLASS. (of this report)			
(12) 11p.		UNCLASSIFIED			
		15a. DECLASSIFICATION/DOWNGRADING SCHEDULE			
16. DISTRIBUTION STATEMENT (of this Report)					
Approved for public release; distribution unlimited.					
17. DISTRIBUTION STATEMENT (of the abstract entered in Block 20, if different from Report)					
18. SUPPLEMENTARY NOTES					
Aerospace Sciences Meeting, 17th, New Orleans, LA, 15-17 Jan 79					
19. KEY WORDS (Continue on reverse side if necessary and identify by block number)					
WALL INTERFERENCE PREDICTION TRANSONIC FLOW AXISYMMETRIC FLOW SMALL DISTURBANCE EQUATIONS					
20. ABSTRACT (Continue on reverse side if necessary and identify by block number)					
A wind tunnel interference assessment concept which presents a rational predictive means of wall interference analysis is evaluated. The procedure consists of employing as an outer boundary condition an experimentally-measured pressure distribution along a convenient control surface located inward from the actual tunnel walls. Attention has been focused on axisymmetric flows in the transonic regime where tunnel interference is high and where the experimentally-measured conditions on the control surface are of mixed subsonic/supersonic type. Based on the transonic small-disturbance equation, results for surface and near flow					

DD FORM 1 JAN 73 1473

UNCLASSIFIED

SECURITY CLASSIFICATION OF THIS PAGE (When Data Entered)

DDC FILE COPY

AD A068767

389783

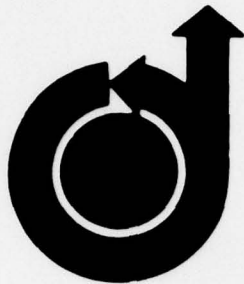
DDC  
RECEIVED  
MAY 22 1979  
B

field pressure distributions are presented for a variety of different slender body shapes. These calculations indicate both the accuracy of the procedure as well as its ease of implementation. The procedure relates directly to the correctable-interference wind tunnel concept recently suggested.

ACCESSION for		
NTIS	White Section	<input checked="" type="checkbox"/>
DDC	Buff Section	<input type="checkbox"/>
UNANNOUNCED		<input type="checkbox"/>
JUSTIFICATION		
BY		
DISTRIBUTION/AVAILABILITY CODES		
Dist.	AVAIL. and/or	SPECIAL
A		

UNCLASSIFIED

**AFOSR-TR- 79 - 0627**



**79-0203**

**A Transonic Wind Tunnel Interference  
Assessment—  
Axisymmetric Flows**

*S.S. Stahara, Nielsen Engineering & Research,  
Mountain View, Ca.; and J.R. Spreiter,  
Stanford University, Stanford, Ca.*

79 05 18 246

**17th AEROSPACE SCIENCES  
MEETING**

**New Orleans, La./January 15-17, 1979**

**Approved for public release;  
distribution unlimited.**

A TRANSONIC WIND TUNNEL INTERFERENCE ASSESSMENT  
- AXISYMMETRIC FLOWS

S. S. Stahara\*  
Nielsen Engineering & Research, Inc.  
Mountain View, California

and  
J. R. Spreiter\*\*  
Stanford University  
Stanford, California

Abstract

A wind tunnel interference assessment concept which presents a rational predictive means of wall interference analysis is evaluated. The procedure consists of employing as an outer boundary condition an experimentally-measured pressure distribution along a convenient control surface located inward from the actual tunnel walls. Attention has been focused on axisymmetric flows in the transonic regime where tunnel interference is high and where the experimentally-measured conditions on the control surface are of mixed subsonic/supersonic type. Based on the transonic small-disturbance equation, results for surface and near flow field pressure distributions are presented for a variety of different slender body shapes. These calculations indicate both the accuracy of the procedure as well as its ease of implementation. The procedure relates directly to the correctable-interference wind tunnel concept recently suggested.

Introduction

The assessment of transonic wind tunnel interference remains an unsatisfactorily resolved problem after almost three decades use of the ventilated tunnel wall concept. The classical homogeneous wall boundary conditions<sup>1</sup> for modeling perforated or porous and slotted walls have proven to be of considerable value for providing insight into the overall effects of ventilated tunnel walls at transonic speeds<sup>2,3</sup>, but as presently constituted, they are seriously deficient for a quantitative study of wall interference. Although the wall characteristics are known to depend on geometrical (test article, tunnel ventilation geometry) as well as flow parameters ( $M_\infty$ ,  $Re$ , local blowing pressure), the exact nature of the wall flow is not adequately known. It has been widely assumed that it is basically viscous in character<sup>4</sup>, although some recent slotted wall results by Berndt<sup>5</sup> indicate that under certain conditions the wall flow for slotted walls may not be completely dominated by viscosity. For porous walls, it has been found<sup>6,7</sup>, that the wall boundary layer can create a nonlinear relationship between velocity normal to the wall and the difference in pressure across the wall. Kacprzyński<sup>8</sup> has demonstrated the feasibility of two-dimensional potential flow calculations using an assumed nonlinear wall characteristic. The present state of development, however, of ventilated wall boundary conditions is such that they are inadequate as a predictive method; namely, they cannot provide a

quantitative a priori assessment of tunnel interference at transonic speeds.

The adaptive wall concept is an attempt to remedy this situation by combining an interference assessment capability together with a tunnel wall modification capability to actually eliminate the interference. Notwithstanding the problems associated with the implementation of adaptive wall technology, the fact remains that many of the currently operating transonic tunnels possess only a limited degree of wall control or none at all. Consequently, the concept of a correctable-interference transonic tunnel recently proposed<sup>9</sup>, and toward which the procedures described in this paper are directly related, appears to have strong merit. The heart of the correctable-interference concept is that the distribution of a single experimentally-measured flow quantity (e.g., pressure or flow angle), obtained along a convenient control surface located sufficiently inward from the actual tunnel walls so as to be removed from local wall disturbances, is employed as an outer boundary condition. This is then used together with a calculative procedure to determine the potential flow about the model interior to the control surface. Comparison of calculated and measured flow quantities at the model surface serve to assess the influence of nonpotential effects (viscosity, rotation); while comparison with a calculated free air flow can provide a quantitative rational assessment of tunnel interference effects.

In this paper we formulate the assessment procedure based on a measured pressure distribution boundary condition, describe its application to axisymmetric transonic flows past a variety of slender bodies, and demonstrate its effectiveness by extensive comparisons with data. The theoretical predictions employ finite-difference SLOR solutions of the axisymmetric transonic small-disturbance potential equation. Results are presented for pressure distributions on the surface and in the near flow field of these various slender bodies at free stream Mach numbers throughout the transonic regime. In order to provide a severe test of the procedure, the particular geometries and flow conditions were purposely selected to be in a range of free stream Mach numbers near one where the tunnel interference is most pronounced, and where the experimentally-measured data on the control surface are of mixed subsonic/supersonic character.

\*Senior Research Scientist, Engineering Management. Member AIAA.

\*\*Professor, Division of Applied Mechanics. Consultant to Nielsen Engineering & Research, Inc. Fellow, AIAA.

## Analysis

### Basic Equations

The coordinate system employed in the analysis is a body-fixed cylindrical system with origin at the nose of the body as illustrated in figure 1.

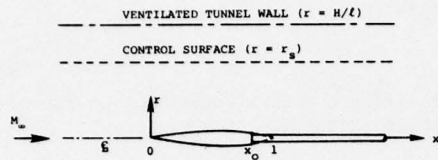


Fig. 1 Illustration of model and tunnel geometry

The flow is assumed to be inviscid and steady, and the body shapes sufficiently slender and smooth that the resulting flow field is irrotational and adequately treated by small-disturbance theory. Accordingly, a disturbance velocity potential  $\phi$  can be defined by

$$\phi(x, r) = U_\infty \ell [x + \phi(x, r)] \quad (1)$$

where  $\phi$  is the total velocity potential,  $U_\infty$  represents the uniform oncoming velocity,  $\ell$  is the complete body length, and the coordinates  $(x, r)$  have been nondimensionalized by  $\ell$ . The governing partial differential equation for  $\phi$  is the usual axisymmetric transonic small-disturbance equation

$$(1 - M_\infty^2 - 1/2 M_\infty^2 (\gamma + 1) \phi_x^2) \phi_{xx} + \frac{1}{r} (r \phi_r)_r = 0 \quad (2)$$

The pressure coefficient in the vicinity of the slender body is given by

$$C_p(x, r) = -2\phi_x(x, r) - \phi_r^2(x, r) \quad (3)$$

With regard to the flow domain indicated in figure 1, the boundary conditions to be imposed on the solution consist of (i) outer flow conditions on the upstream, downstream and lateral boundaries which are appropriate to the behavior of the body in a free-air or wind tunnel environment, (ii) the body surface condition of no normal flow, and (iii) shock wave conditions to be applied at any shock surface appearing in the flow such that the potential is continuous through the shock and the velocity components satisfy the small-disturbance approximation to the Rankine-Hugoniot conditions at the location of the shock. The appropriate outer flow boundary conditions are discussed in the following section. The requirements on the body and shock surface lead to the following conditions on  $\phi$

$$\lim_{r \rightarrow 0} (r \phi_r) = \frac{S'(x)}{2\pi} \quad (4)$$

$$\begin{aligned} [\phi]_{\text{shock}} &= 0; \left[ r(1 - M_\infty^2 - M_\infty^2 (\gamma + 1) \phi_x^2) \phi_{xx} \right]_{\text{shock}} = 0 \\ [\phi_x^2] + [r \phi_r^2]_{\text{shock}} &= 0 \end{aligned} \quad (5)$$

where  $S(x)$  is the body cross sectional area distribution nondimensionalized by  $\ell^2$ , and the symbols

$[\ ]$  and  $\langle \rangle$  signify the difference and the mean, respectively, of the enclosed quantity on the two sides of the shock surface.

### Outer Boundary Conditions

The outer boundary condition to be applied along the cylindrical control surface indicated in figure 1 is determined from static pressure measurements. The actual condition imposed on  $\phi$  is of Dirichlet type, and is given by

$$\phi(x, r_s) = -1/2 \int_{x_1}^x C_{pm}(\xi, r_s) d\xi + \phi(x_1, r_s) \quad (6)$$

where  $r_s$  denotes the radial location of the control surface,  $x_1$  the position of the upstream boundary, and  $C_{pm}$  the measured pressure coefficient along  $r_s$ . The quantity  $\phi(x_1, r_s)$ , which is proportional (to within a constant) to the average flow inclination at the upstream boundary, has for convenience and without loss of generality been set to zero. Along the upstream and downstream boundaries, for subsonic oncoming flow we have employed the conditions

$$M_\infty < 1: \phi(x_1, r) = 0; \phi(x_N, r) = \phi(x_N, r_s) \quad (7)$$

while for sonic and supersonic oncoming flow, we have used the uniform flow conditions

$$M_\infty \geq 1: \phi(x_1, r) = \phi_x(x_1, r) = 0; \phi_x(x_N, r) = 0 \quad (8)$$

While, strictly speaking, for  $M_\infty > 1$ , no condition is required at the downstream boundary if as we assume it is sufficiently far removed so that the outflow is entirely supersonic. For actual numerical application, however, some condition is needed<sup>3</sup> to treat subsonic outflow which may develop during the course of the relaxation solution process prior to convergence. From numerical experimentation, the condition  $\phi_x = 0$  given in equation (8) has been found to be satisfactory. These conditions are summarized in figure 2.

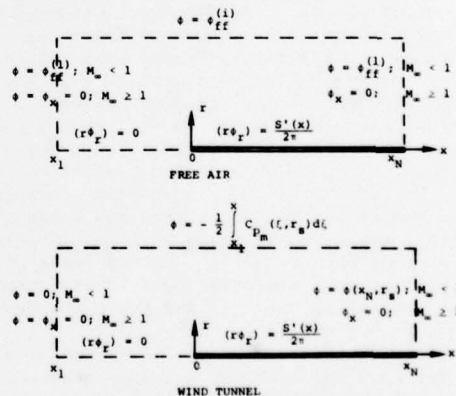


Fig. 2 Summary of boundary conditions for free air and wind tunnel environment

For the corresponding comparative free air calculations, we have employed the following conditions. For  $M_\infty < 1$  flows, the asymptotic far-field solution  $\phi_{ff}$  given by an axisymmetric source and axisymmetric doublet<sup>10</sup> is employed on all the outer boundaries, i.e.

$$\phi_{ff}^{(1)}(x, r) = \frac{-S_0}{2\bar{r}} + 1/4 [-S_0 + 2 \int_0^{x_0} S(\xi) d\xi + M_\infty^2(\gamma + 1) \int_{-\infty}^{\infty} \int_0^{\infty} \phi_x^2(\xi, r) r dr d\xi] \cdot \frac{\bar{x}}{r^3} \quad (9)$$

where  $r = (\bar{x}^2 + (1 - M_\infty^2)r^2)^{1/2}$ ,  $\bar{x} = x - 1/2$ ,  $x_0$  is the location of the body base, and  $S_0$  is either the base area of the body or that of a sting attached to the body base nondimensionalized by  $\ell^2$ . On the lateral boundary, for  $M_\infty = 1$  flows, we employ the asymptotic solution<sup>11</sup>

$$\phi_{ff}^{(2)}(x, r) = \frac{f(x/r^{4/7})}{r^{2/7}} \quad (10)$$

while for  $M_\infty > 1$ , the following relation<sup>12</sup> is used

$$\phi_{ff}^{(3)}(x, r) = f(x - \sqrt{M_\infty^2 - 1} r - \frac{M_\infty^2(\gamma + 1) \cdot r \phi_x}{\sqrt{M_\infty^2 - 1}}) / \sqrt{r} \quad (11)$$

On the upstream and downstream boundaries, for  $M_\infty \geq 1$ , the conditions given in equation (8) are employed. These conditions are also summarized in figure 2.

#### Computational Procedure

The method employed for the solution of equation (2) is a finite-difference successive line over-relaxation (SLOR) procedure using Murman-Cole type-dependent difference operators<sup>13</sup>. To realize the calculation, we have employed the following fully-conservative form

$$[\eta(K\bar{\phi}_x - 1/2\bar{\phi}_x^2)]_x + [\eta\bar{\phi}_\eta]_\eta = 0 \quad (12)$$

where

$$\bar{\phi}(x, \eta) = \phi(x, r)/\tau^2; K = (1 - M_\infty^2)/\tau^2 M_\infty^2(\gamma + 1); \eta = \tau M_\infty \sqrt{\gamma + 1} r \quad (13)$$

and  $\tau$  denotes the thickness ratio of the body. The finite difference form of the equation actually solved is that suggested by Jameson<sup>14</sup> in terms of a correction potential. Additionally, a pseudo-time term of the form  $-\epsilon \frac{\partial \phi}{\partial x} \phi_{xt}$  was added to enhance stability and speed convergence.

#### Results

In order to examine the feasibility of the procedure described above for assessing tunnel interference, as well as to examine the stability and convergence characteristics of the computational method subject to the experimentally-imposed Dirichlet condition of equation (6), we have extensively tested the method using data obtained in a conventional transonic tunnel on five different slender body shapes and at Mach numbers at and near one. The particular geometries and flow conditions were purposely selected to study situations where tunnel interference is most pronounced, and insofar as possible where the experimentally-measured data on the control surface are of mixed subsonic/supersonic character.

The body shapes examined are (i) parabolic-arc<sup>15</sup>, (ii) power-law body with  $S_{\max}$  at  $x = 0.3^{15}$ , (iii) power-law body with  $S_{\max}$  at  $x = 0.7^{15}$ , (iv) parabolic-arc with bumpy midsection<sup>16</sup>, and (v) parabolic-arc with indented midsection<sup>16</sup>. Geometric details of these shapes are provided in figure 3. Data for all of these bodies were obtained in the Ames 14-foot transonic wind tunnel.

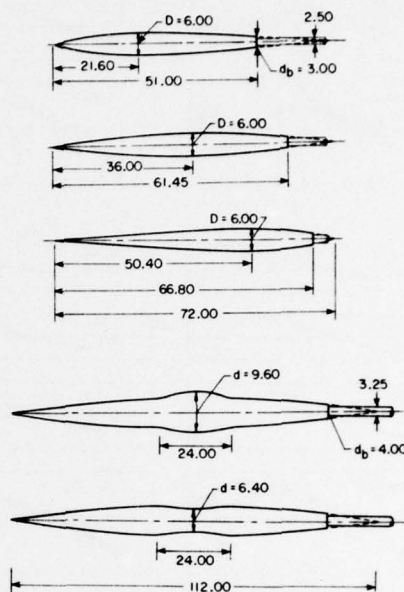


Fig. 3 Geometric details of various wind tunnel models considered with dimensions in inches

#### Smooth Bodies

In figure 4 we have displayed comparisons of the theoretical results with data<sup>15</sup> for a parabolic-arc body of revolution having a diameter to complete body length  $D/\ell = 12$ . Results are shown at free-stream Mach numbers  $M_\infty = 0.975, 1.00, 1.025$ , and  $1.10$ . For the particular body tested the tunnel half-height to complete body length ratio was  $H/\ell = 7/6$ . The theoretical results indicated by the solid lines (—) represent SLOR solutions of equation (12) employing the measured pressure distribution outer boundary condition equation (6). Pressure survey data obtained at the radial location  $r/D = 4$ , which represents the outermost survey station at which data were taken, were used. The results indicated by the dashed lines (---) represent the corresponding theoretical results for free air conditions, equations (9-11).

The theoretical body surface pressure coefficients were determined by extrapolating the SLOR results obtained along the first radial grid line  $r_1$  down to the body surface according to the slender body result

$$C_p(x, R) = - \left[ 2\phi_x(x, r_1) + \frac{S''(x)}{\pi} \ln \left( \frac{R}{r_1} \right) + \left( \frac{dR}{dx} \right)^2 \right] \quad (14)$$

where  $R$  is the equivalent body radius. The flow field pressures were calculated by bi-linear inter-

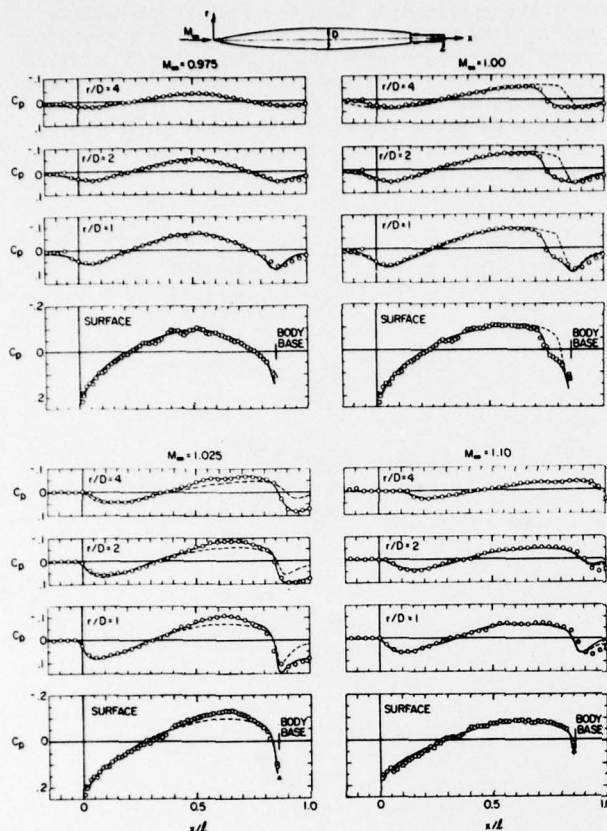


Fig. 4 Experimental<sup>15</sup> (○) and theoretical (—) pressure distributions for a parabolic-arc body with  $D/\ell=1/12$  at several transonic Mach numbers; —  $C_{pm}(r/D=4)$  input, --- free air

polation for  $\phi$  through the flow field grid, and then employing equation (3) to calculate the pressure coefficient. The  $(x,r)$  mesh density used for the imposed pressure distribution calculations was  $(80 \times 24)$  with 40 equally-spaced points on the body. The  $r$ -grid as well as the  $x$ -grid ahead and behind the body were expanded geometrically using a grid ratio of 1.2:1. The  $x$ -mesh extended 2 body lengths ahead and 2 body lengths behind the body. The location of the first  $r$ -grid line was at  $r = D/2\ell$  and the control surface was at  $r_s = 1/3$ . For the free air calculations, an identical  $x$ -mesh was used and a 40 point  $r$ -grid was employed that was identical to the previous  $r$ -mesh out to  $r = 1/3$  but which was continued laterally out to  $r = 5$ . In numerically implementing the imposed pressure distribution boundary condition equation (6), it was necessary to extend the data<sup>15,16</sup> to the upstream and downstream boundaries, since the experimental pressures were only obtained for  $-0.15 < x/\ell < 1.0$ . In addition, numerical experimentation indicated that some degree of data point smoothing was desirable. Because the data sometimes contained one or more shock waves, however, and the faithful reproduction of those shock profiles was considered essential, the method selected was a least squares smoothing spline fit with individual point weighting. As can be seen in figure 4 as well as in the results to follow, this produced extremely satisfactory results in all cases considered. In the

SLOR solution process, relaxation factors  $1.7 < \omega < 1.9$  were used and the coefficient of the pseudo-time term was set to  $\epsilon = 0.5$ . No stability problems were encountered and convergence in all of the imposed pressure distribution cases was very rapid, with a  $|\Delta\phi|_{\max} < 10^{-5}$  criteria reached within 75 iteration sweeps. Pressure changes on the body usually become less than  $10^{-4}$  before 40 iterations. The corresponding results for the free air calculations generally required about 25% more iteration cycles to reach the same convergence level.

With regard to the comparisons in figure 4, we note that the agreement between the data and the imposed pressure-condition theoretical results is excellent for both surface and flow field pressures. The location and strengths of shocks are accurately predicted throughout this flow-sensitive Mach number range. Viscous effects on these flows, which have Reynolds numbers based on body length of approximately 24 million, appear to be quite small and confined to the flow immediately behind the body base where the step-down sting results in a separated flow situation. The corresponding free air results are interesting in that they indicate essentially no tunnel interference at  $M_\infty = 0.975$ , a substantial amount at  $M_\infty = 1.00$  and  $1.025$ , and then very little again at  $M_\infty = 1.10$ . This serves to point out the narrowness of the critical range for this class of smooth slender bodies.

Figure 5 presents analogous results for a slender body having the same maximum diameter to length ratio ( $D/\ell=1/12$ ) as the parabolic-arc body of figure 4, but with the location of maximum diameter at 30% of the body length. The ordinates of this body are given by

$$R = A [(1-x) - (1-x)^n] \quad (15)$$

where  $n = 6.03$  and  $A$  is related to  $D/\ell$  and  $n$  by

$$A = \left[ n^{n/(n-1)} / 2 (n-1) \right] (D/\ell) \quad (16)$$

As in the case of the parabolic-arc body, comparisons of the  $C_{pm}$ -input theoretical results with data again display excellent agreement. The corresponding free air comparisons indicate that the tunnel interference effects are more pronounced for this shape than for the parabolic-arc. This is to be anticipated and is in accord with the observations noted in reference 17 that, for a given thickness ratio and length, wave reflection interference on the afterbody region increases as the point of maximum thickness moves forward.

We note for this body that the  $M_\infty = 0.975$  results display only slight interference, while the  $M_\infty = 1.00$  comparisons indicate strong tunnel interference which has resulted in a shock movement on the body surface of approximately 15% of the body length. For the  $M_\infty = 1.025$  results, the measured boundary condition was imposed at  $r/D = 3$  rather than 4, since  $r/D = 4$  data were not obtained for this flow. We observe that the comparison of the predicted result with data is quite good, in particular, even for the flow field pressures at  $x$  locations behind the body base. Only for the  $M_\infty = 1.10$  case does a slight discrepancy arise, and that only for the flow field results at locations

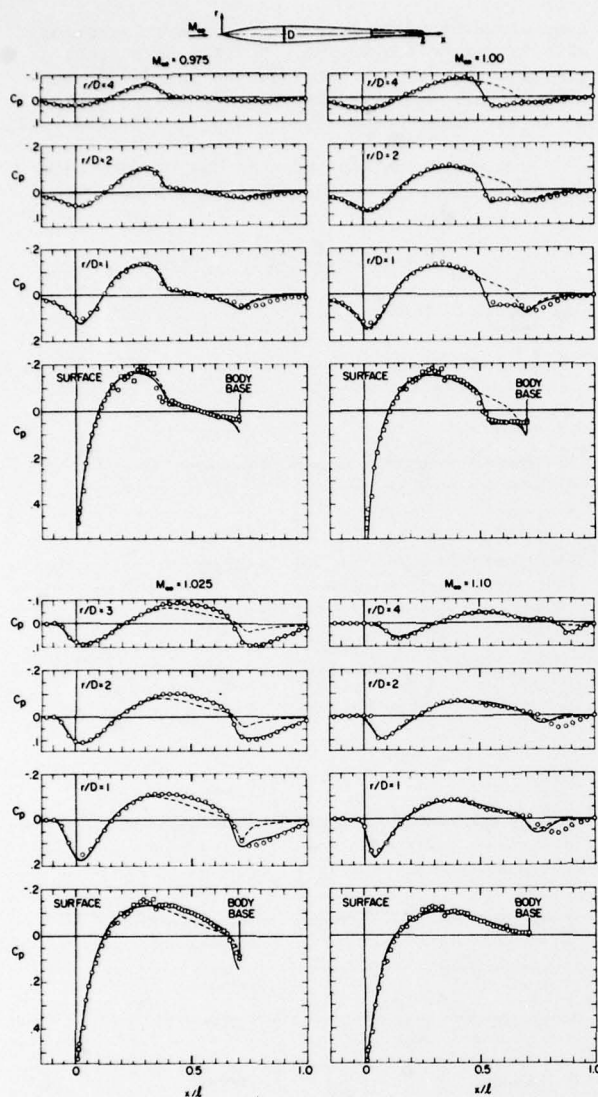


Fig. 5 Experimental<sup>15</sup> ( $\circ$ ) and theoretical (---) pressure distributions for a body with maximum thickness at  $x/l=0.3$  and  $D/l=1/12$  at several transonic Mach numbers:  
—  $C_{pm}$  ( $r/D=4$ ) input, --- free air

behind the body base. This may be caused by the interaction of an oblique shock emanating from the body base and interacting with the separated base flow. A more modest indication of this can be observed in the corresponding results at  $M_\infty = 1.10$  for the parabolic-arc body shown in figure 4.

The next set of results displayed in figure 6 are for a similar shape but with the maximum diameter located at  $x = 0.70$ . The ordinates for this shape are given by

$$R = A [x - x^n] \quad (17)$$

with  $n = 6.03$  and  $A$  given by equation (16). Again the  $C_{pm}$ -input theoretical predictions are in very good agreement with the data. The free air results indicate, however, as may have been anticipated from the comparisons given in figure 4 and 5, that

tunnel interference for this shape is very small, and restricted essentially to the  $M_\infty = 1.00$  results at axial locations behind  $x = 0.90$ .

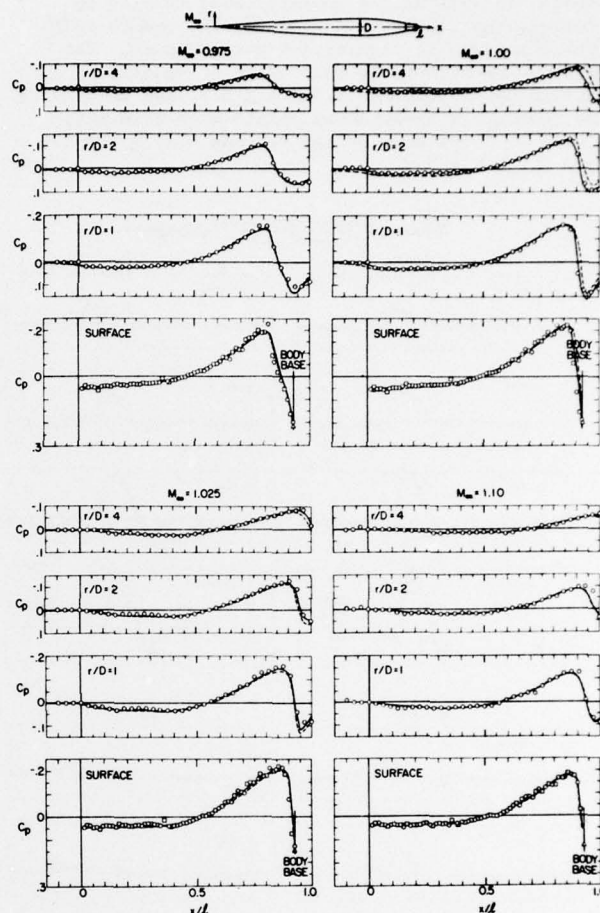


Fig. 6 Experimental<sup>15</sup> ( $\circ$ ) and theoretical (---) pressure distributions for a body with maximum thickness at  $x/l=0.7$  and  $D/l=1/12$  at several transonic Mach numbers;  
—  $C_{pm}$  ( $r/D=4$ ) input, --- free air

#### Bumpy and Indented Bodies

In order to provide an indication of the ability of the method to handle situations where multiple shocks or several high gradient regions exist on the control surface, we have examined the bumpy and indented bodies<sup>16</sup> which were tested transonically in the Ames 14-foot wind tunnel. These bodies were quite long ( $l = 112$  inches - see figure 3), and consisted of basic parabolic-arc bodies having maximum diameter to length ratios  $D/l = 14$  but with a sinusoidal bump or indentation centered about the body midpoint and extending over  $0.393 \leq x \leq 0.607$ . The ordinates of the shapes are given by

$$R = (2 D/l) (x - x^2) \pm \left( \frac{D}{10l} \right) \sin^2 \left[ \frac{\pi (x - x_1)}{(x_2 - x_1)} \right] \quad (18)$$

where  $(x_1, x_2) = (0.393, 0.607)$ .

The results indicated in figure 7 are for the bumpy body. In the SLOR calculation of these results, as well as the indented body results to follow, the same r-grid used for the smooth body results given in figures 4-6 was employed. The x-grid was refined by clustering 40 equally-spaced points between  $0.3 \leq x \leq 0.7$ , and then using 30 geometrically-expanded points with grid ratio 1.2:1 to cover each of the regions  $-2.0 \leq x \leq 0.3$  and  $0.7 \leq x \leq 3.0$ .

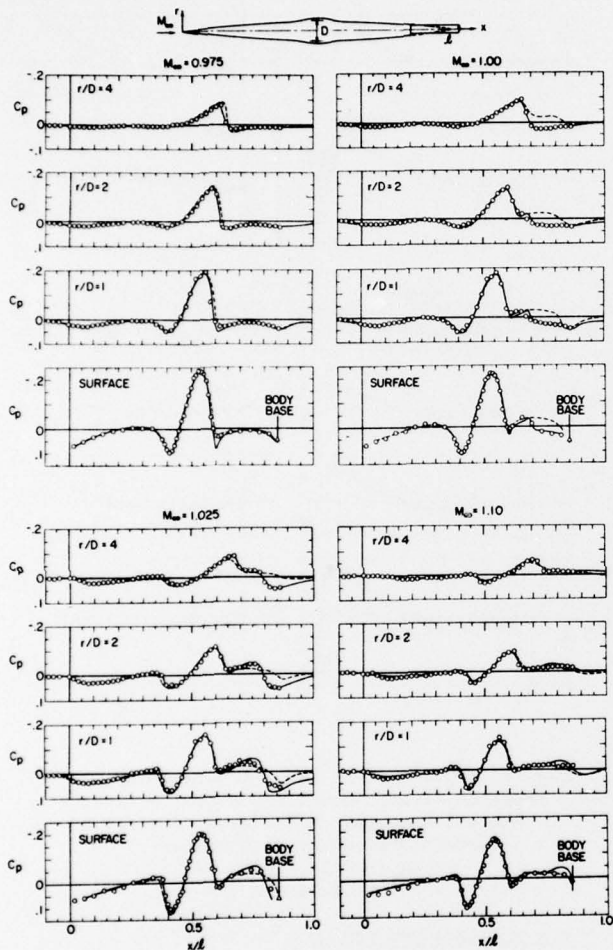


Fig. 7 Experimental<sup>16</sup> (○) and theoretical (---) pressure distributions for a bumpy parabolic-arc body with  $D/l=1/14$  at several transonic Mach numbers; —  $C_{pm}(r/D=4)$  input, --- free air

With regard to the results indicated in figure 7, the experimental flow field pressures at the radial location  $r/D = 4$ —the outermost station at which data were taken—display much steeper gradients than any of the smooth body data shown in figures 4-6. In addition, the data at  $M_\infty = 1.025$  and  $1.10$  indicate multiple regions of rapid compression. Comparison with the theoretical  $C_{pm}$ -input results displays very good agreement at all the Mach numbers. Some quite minor discrepancies are evident in the region behind the

bump where boundary layer-shock wave interaction effects may have occurred. The free air results indicate that tunnel interference exists for this shape at all the Mach numbers shown, with the strongest interference again at  $M_\infty = 1.00$  and  $1.025$ .

The corresponding indented body results displayed in figure 8 on the other hand show a very

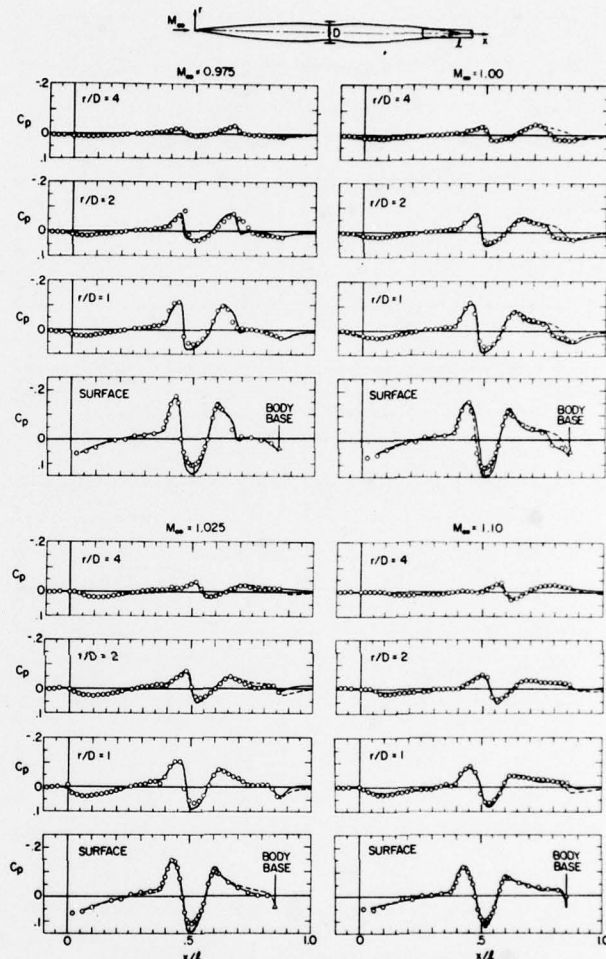


Fig. 8 Experimental<sup>16</sup> (○) and theoretical (---) pressure distributions for an indented parabolic-arc body with  $D/l=1/14$  at several transonic Mach numbers; —  $C_{pm}(r/D=4)$  input, --- free air

small tunnel effect at every free stream Mach number other than  $M_\infty = 1.00$ . The body indentation apparently significantly reduces the size and strength of the supersonic pockets for  $M_\infty < 1$ , and similarly, the subsonic pockets at  $M_\infty > 1$ . In fact, at  $M_\infty = 1.025$  and  $1.10$  the flow at  $r/D = 4$  is purely supersonic. We note that, for all of the cases shown, the theoretical results for both free air and  $C_{pm}$ -input indicate a higher pressure peak at the body midpoint than the data. This is undoubtedly due to a thickened boundary layer in the indented region caused by the decelerating flow. This effectively results in a shallower and milder indentation and consequent smaller pressure peak.

### Effect of Control Surface Location

The final results shown in figure 9 display the effect on the predicted surface and near flow field pressures of varying the radial location of the control surface at which the experimentally-measured boundary condition is imposed. These

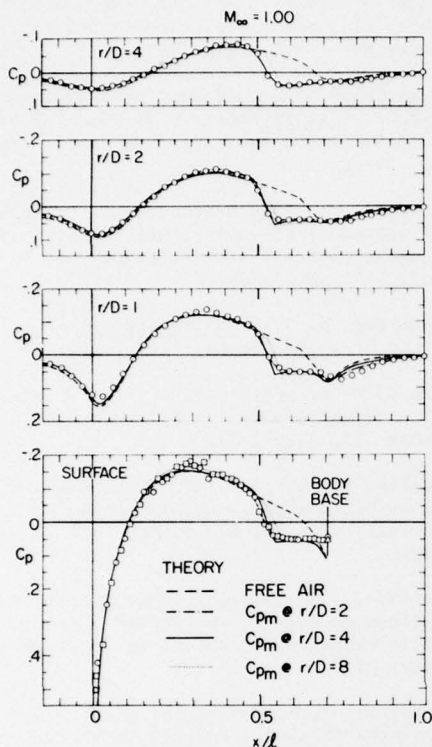


Fig. 9 Effect of control surface location on near flow field and body surface theoretical pressure distributions at  $M_\infty = 1.00$  for the  $(x/l)_{R_{max}} = 0.3$  body shape

results are for the  $(x)_{R_{max}} = 30\%$  body at  $M_\infty = 1.00$ , for which comparisons were previously shown in figure 5. This example was purposely selected for its strong tunnel interference characteristics as well as the fact that experimental flow field pressures were obtained for this flow out to the radial location  $r/D = 8$ . The dashed (---) and solid (—) lines in figure 9 correspond as before to theoretical results for free air and  $C_{pm}$ -input at  $r/D = 4$ . The dash-dot (-.-) and dotted (···) lines correspond to theoretical results for  $C_{pm}$ -input at  $r/D = 2$  and 8. For the results with  $C_{pm}$ -input at  $r/D = 2$ , the predicted pressures on the body surface and at  $r/D = 1$  are essentially indistinguishable from the data everywhere, and in particular in the vicinity of the shock wave. The  $C_{pm}$ -input at  $r/D = 4$  results are also quite satisfactory and differ but slightly from the  $r/D = 2$  results only near the shock. For the  $C_{pm}$ -input at  $r/D = 8$ , a consistent discrepancy in the shock positions for both the surface and flow field pressures that amounts to approximately 3-4% of body length is observed, however. The flow survey location at  $r/D = 8$  is slightly more than halfway ( $4/7 H/l$ ) from the tunnel centerline to the closest point on the tunnel walls. For these results it is likely that the non-axisymmetric effects of the square tunnel

configuration are the cause of the discrepancy. If the tunnel cross section were cylindrical, the radial location of the control surface could probably be taken closer to the wall without loss of accuracy to the interior calculation. The important point of these results, however, is they demonstrate that, for any test model/tunnel configuration, there will always exist a minimum distance from the tunnel walls, closer than which it is inappropriate to obtain outer boundary data. Within that minimum distance from the wall, factors such as tunnel flow nonuniformities, local wall disturbances, etc. will tend to wash out the accuracy of the experimental measurements with a subsequent detrimental effect on the theoretical calculations.

### Potential Utility

The ultimate utility of any wall interference assessment procedure is in the evaluation and re-interpretation of data obtained in a wind tunnel to corresponding free air conditions. Toward that end there are several interesting options in which the present procedure can be used. For the results reported, we have employed the assessment procedure primarily for the observation of two separate effects present in the data, viz: (1) nonpotential effects of viscosity and rotation, and (2) wind tunnel interference. Nonpotential effects were evaluated by noting the difference between the data and the theoretical prediction with  $C_{pm}$ -input, while the difference between the theoretical free air calculation and that with  $C_{pm}$ -input provided a measure of the tunnel interference present. While these two calculations in themselves do not reinterpret the data to free air conditions, they serve to identify the range of test conditions where tunnel interference is minimum for a specific test article. Such information is of major importance for existing conventional transonic tunnels where wall control is limited or impossible, and relates to "the principle of minimizing interference rather than corrections"<sup>18</sup>.

For the actual correction or reinterpretation of the test data to free air conditions, Kemp<sup>9</sup> has suggested an iterative procedure which effectively corrects the tunnel data through corrections to the oncoming uniform flow. The first step of the method uses the above predictive method and consists of solving the potential flow problem using the experimentally-measured boundary condition. This calculation yields the theoretical body surface velocity distribution  $(\phi_s)_m$ . Next, the corresponding free air potential solution is obtained which provides the surface velocity  $(\phi_s)_{FA}$ . The difference criteria  $|(\phi_s)_m - (\phi_s)_{FA}| < \epsilon$  is then examined along the entire surface, and the data classified as negligible, correctable, or uncorrectable (a judgement). If correctable, the free air problem is recomputed in an iterative sequence which, for the axisymmetric flows considered here, consists of changing the oncoming Mach number. When the difference criteria is satisfied, the tunnel data are interpreted as free air data at the new Mach number. For the three-dimensional case, corrections in oncoming flow angle would enter the iterative process as well.

### Concluding Remarks

An evaluation has been made of a wind tunnel interference assessment concept which employs an experimentally-measured pressure distribution obtained along a convenient control surface as an outer boundary condition. Based on the axisymmetric transonic small-disturbance equation, extensive calculations have been made for a number of slender bodies at Mach numbers in the transonic regime. Particular emphasis was placed on flows with oncoming Mach numbers at and near one where tunnel interference was high and where the experimentally-measured conditions on the control surface were of mixed subsonic/supersonic character. For all of the cases studied, the implementation of the measured boundary condition in Dirichlet form in the numerical procedure proved stable and no convergence problems were encountered. The predicted body surface and near flow field pressure results have been compared with data and with corresponding theoretical free air calculations. The comparisons with data display very good agreement, capturing the location and strengths of surface and flow field shocks; while the free air comparisons provide the basis for a quantitative evaluation of wind tunnel interference. From these results we conclude that such a procedure can be useful as a practical wall correction method for moderately-variable or fixed geometry transonic wind tunnels where alteration of the tunnel wall is limited or impossible.

### Acknowledgement

The results reported are based on research partially supported by the Air Force Office of Scientific Research under Contract No. F44620-75-C-0047 and by the U.S. Army Research Office under Contract No. DAAG29-77-C-0038.

### References

1. Baldwin, B., Turner, J., and Knechtel, E.: Wall Interference in Wind Tunnels with Slotted and Porous Boundaries at Subsonic Speeds. NASA TN 3176, 1954.
2. Bailey, F. R.: Numerical Calculation of Transonic Flow About Slender Bodies of Revolution. TN D-6582, 1971, NASA.
3. Murman, E. M.: Computation of Wall Effects in Ventilated Transonic Wind Tunnels. AIAA Paper 72-1007, Sept. 1972.
4. Anon.: Report of the AGARD ad hoc Committee on Engine Airplane Interference and Wall Corrections in Transonic Wind Tunnel Tests. AGARD-AR-36-71, Aug. 1971.
5. Berndt, S. B.: Inviscid Theory of Wall Interference in Slotted Test Sections. ICAS Paper No. 76-03, Oct. 1976.
6. Chew, W. L.: Cross-Flow Calibration at Transonic Speeds of Fourteen Perforated Plates with Round Holes and Airflow Parallel to the Plates. AEDC-TR-54-65, July 1955.
7. Vidal, R. J., Erickson, J. C., Jr. and Catlin, P. A.: Experiments with a Self-Correcting Wind Tunnel. AGARD-CP-174, Wind Tunnel Design and Testing Techniques, pp. 11-1 to 11-13, Oct. 1975.
8. Kacprzynski, J. J.: Transonic Flow Field Past 2-D Airfoils Between Porous Wind Tunnel Walls with Nonlinear Characteristics. AIAA Paper No. 75-81, Jan. 1975.
9. Kemp, W. B., Jr.: Toward the Correctable-Interference Transonic Wind Tunnel. Proc. AIAA 9th Aerodynamic Testing Conf., June 1976, pp. 31-38.
10. Krupp, J. A., and Murman, E. M.: Computation of Transonic Flows Past Lifting Airfoils and Slender Bodies. AIAA Journal, Vol. 10, No. 7, July 1972, pp. 880-886.
11. Guderley, K. G.: The Theory of Transonic Flow. Pergamon Press, Mass., 1962.
12. Cheng, H. K. and Hafez, M. M.: On Three-Dimensional Structure of Transonic Flows. USCAE 121, July 1972.
13. Murman, E. M.: Analysis of Embedded Shock Waves Calculated by Relaxation Methods. AIAA Journal, Vol. 12, No. 5, May 1974, pp. 626-633.
14. Jameson, A.: Transonic Flow Calculation. Lecture Series 87, von Karman Institute for Fluid Dynamics, Computational Fluid Dynamics, March 1976.
15. McDevitt, J. B. and Taylor, R. A.: Pressure Distributions at Transonic Speeds for Slender Bodies Having Various Axial Locations of Maximum Diameter. NACA TN 4280, 1958.
16. Taylor, R. A.: Pressure Distribution at Transonic Speeds for Bumpy and Indented Mid-sections of a Basic Parabolic-Arc Body. NASA Memo. 1-22-59A, 1959.
17. Spreiter, J. R., Smith, D. W., and Hyett, B. J.: A Study of the Simulation of Flow with Free Stream Mach Number 1 in a Choked Wind Tunnel. NACA TR R-73, 1960.
18. Berndt, S. B.: On the Influence of Wall Boundary Layers in Closed Transonic Test Sections. FFA Rept. 71, 1957.